Catalysis Letters (2018) 148:3502–3513
https://doi.org/10.1007/s10562-018-2546-6

Selective CO Methanation Over Ru Supported on Carbon Spheres: The Effect of Carbon Functionalization on the Reverse Water Gas Shift Reaction

David O. Kumi[1] · Mbongiseni W. Dlamini[1] · Tumelo N. Phaahlamohlaka[1] · Sabelo D. Mhlanga[2] · Neil J. Coville[1] · Mike S. Scurrell[3]

Received: 17 August 2018 / Accepted: 6 September 2018 / Published online: 22 September 2018
© Springer Science+Business Media, LLC, part of Springer Nature 2018

Abstract

Mesoporous carbon spheres (CSs-H) were hydrothermally synthesised using sugar as carbon source. The as-synthesized CSs-H was microporous but after thermal treatment at 900 °C for 4 h it became mesoporous (surface area of 463 $m^2\ g^{-1}$). Further treatment of the annealed CSs-H with HNO_3 gave a functionalized CSs-H with a high defect content in the carbon matrix which resulted in an increase in surface area (509 $m^2\ g^{-1}$). The functionalized and un-functionalized CSs-H were used to support nano Ru particles for CO, CO_2 and selective CO methanation reactions. The Ru supported catalysts were prepared using both impregnation and microwave polyol synthesis methods. It was evident from the reduction studies that the functional groups on the surface of the CSs-H influenced the reduction of the RuO_2 to Ru. The catalyst with smaller and well dispersed RuO_2 particles ($d = 2.7$ nm) (prepared by the microwave polyol technique) gave a high activity in both CO and selective CO methanation studies. The larger Ru particles observed on the un-functionalized CSs-H showed poor activity for CO and selective CO methanation reactions and also did not promote the reverse water gas shift reaction.

Graphical Abstract

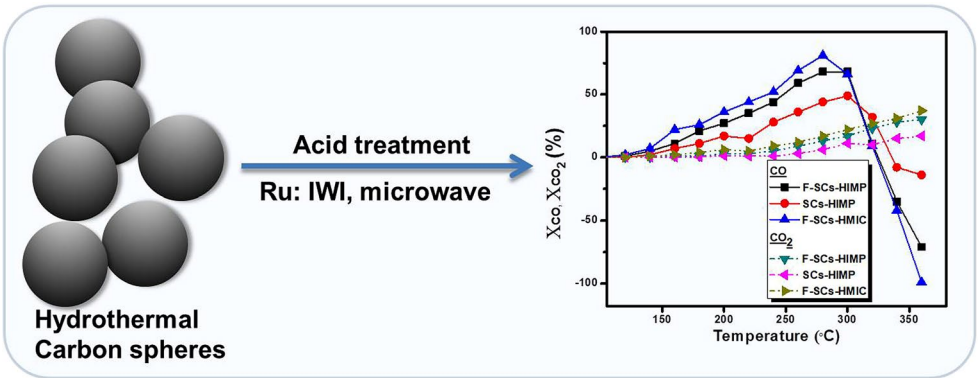

Keywords CSs-H · Mesoporous · Functional groups · Selective CO methanation · Ruthenium

1 Introduction

Hydrogen is an alternative to fossil fuel for generating thermal or electric energy and can be fed directly into fuel cells to generate electric power cleanly. Hydrogen is among the most abundant elements on earth and it is generally produced from catalytic reforming of hydrocarbons followed by

Electronic supplementary material The online version of this article (https://doi.org/10.1007/s10562-018-2546-6) contains supplementary material, which is available to authorized users.

Extended author information available on the last page of the article

the water gas shift reaction (WGS). This secondary hydrogen production process (WGS) leaves the H_2 rich feed with ~ 1% carbon monoxide. The CO in this H_2 rich feed is regarded as a major setback because this concentration of the CO is high enough to poison the anode catalyst of a polymer electrolyte fuel cell (PEMFC). The anode is usually made of Pt or a Pt-alloy and a maximum CO concentration that is permissible for use in fuel cells is 10 ppm for Pt electrodes and 50 ppm for Pt-alloy electrodes [1–3].

The preferential oxidation of CO in a H_2-rich gas (Eq. 1) has been the most effective approach to address this problem of the removal of CO [4–6]. However, there are some severe limitations that have generated interest in finding alternatives to this process. These limitations include the challenge of supplying the appropriate amount of oxygen (or air) needed from external sources into the PROX chamber, designing a cooling system, and an oxygen (or air) and hydrogen-rich gas mixer component, all making the technique complicated and costly. The addition of oxygen (or air) gives rise to hydrogen dilution, which restricts the operation parameters of the PEMFCs further, hampering its application in the transportation industry [2, 7–10]. The challenges experienced in the PROX reaction can be circumvented through the use of selective CO methanation (Eq. 2). Both reactants necessary for the methanation reaction (CO and H_2) are present in the reformate gas feed and the methane generated in the process is inert and can be utilized in the afterburner [7, 11, 12].

The methanation of CO_2 (Eq. 3) and the reverse water gas shift reaction [RWGS (Eq. 4)], which are undesired reactions, can occur if the reaction conditions and the catalyst are not carefully chosen. Both of these reactions result in the consumption of large quantities of H_2. Efforts have thus been made to design a catalyst with high activity at sufficiently low temperatures to overcome the CO_2 methanation and RWGS reactions.

$$CO + (1/2)O_2 \leftrightarrow CO_2; \quad \Delta H^\circ 298 = -284 \text{ kJ/mol} \tag{1}$$

$$CO + 3H_2 \leftrightarrow CH_4 + H_2O \quad \Delta H^\circ 298 = -206 \text{ kJ/mol} \tag{2}$$

$$CO_2 + 4H_2 \leftrightarrow CH_4 + 2H_2O \quad \Delta H^\circ 298 = -165 \text{ kJ/mol} \tag{3}$$

$$CO_2 + H_2 \leftrightarrow CO + H_2O \quad \Delta H^\circ 298 = 41 \text{ kJ/mol} \tag{4}$$

The above reactions are all catalysed by a range of metals and these metals are supported to enhance their activity. Numerous studies have revealed that the nature of a support can alter the dispersion and the surface area of the catalytically active species. These studies have affirmed the crucial role played by a catalyst support material in immobilizing the active phase species against the loss of surface area via sintering which can influence the overall activity of the catalyst [13–15].

Recent studies have focused on exploring mesoporous materials as catalyst supports which stabilize the metal/metal oxide species within the mesopores. This approach has been used to address the sintering of the active metal species [16]. To a large extent, the catalytic performance can be connected to the effective loading of the metal species into the pore network of the mesopores. Mesoporous supports tend to provide easy accessibility to the dispersed active metal species [17]. High dispersions have been reported when nickel or noble metal nanoparticles are loaded into an aluminum oxide framework via in situ metal ion incorporation [1, 18–21]. The active centers tend to be isolated from each other and this enhances their catalyst sinter resistance [18].

Another approach to support metal particles for use in selective CO methanation is to use carbon supports. Selective CO methanation studies on carbon based supported catalysts have focused on the use of carbon nanotubes (CNTs) and carbon nanofibers (CNFs) [22–30] with fewer studies reported on the use of carbon spheres (CSs). Similar properties might be expected when CNFs, CNTs or CSs are used as catalyst support materials. However, studies have revealed that typical synthesis methodologies to produce CNFs and CNTs do not remove all the catalyst used to make the carbons, even after acid treatment [31]. The exact effect of the residual catalyst on a catalyse reaction is difficult to quantify. CSs on the other hand are made without the use of a catalyst and so metal purification issues are not a problem. Different facile routes have been established to synthesize CSs, and these include the chemical vapour deposition technique [32] and the hydrothermal technique [33]. Further, the advantages known to be associated when using CNTs and CNFs as catalyst supports such as high surface area and easy surface functionalization apply to CSs as well.

Studies from Tada et al. showed that OH groups that are present on a catalyst support promotes CO_2 hydrogenation [34]. Other studies have suggested that CO_2 interacts with the surface support which leads to carbonate specie formation on the support, which then converts into formate species via hydrogen spill over. The formate species bordering on the active metal are then decomposed into CO at the metal-support interface leaving the residual species on the support. The CO adsorbs on the active metal surface and finally reacts with H_2 to form CH_4. In contrast, the CO interacts with the surface of the active metal species [35, 36]. This implies that the design of a catalyst with less fuctional groups that facilitate adsorption of CO_2 could reduce CO production or reduce the RWGS reaction (Eq. 3).

Herein, we have employed hydrothermally synthesized CSs with known high surface areas and well-structured pores [33] as a catalyst support for Ru in the selective CO methanation reaction. The CS surface was modified by acid treatment (HNO_3) which introduced functional groups such as COOH and OH species onto the surface [37, 38]. This

permitted a study of the effect of the surface groups on the selective CO methanation reaction. A catalyst was also prepared without acid functionalizing the surface of the CSs to study the effect of functional groups on the RWGS reaction. As far as we are aware, this is the first report on the behaviour of Ru-carbon sphere catalysts for the methanation of carbon oxides.

2 Experimental

2.1 Hydrothermal Synthesis of Carbon Spheres (UN-CSs-H)

The hydrothermal approach was employed to synthesize the carbon spheres [32, 39]. The carbon source used was sucrose. The experiment was conducted using a 0.3 M aqueous sucrose solution, added into a Teflon vessel (90% filling ratio) with a total volume of 90 mL. The vessel and its contents were placed in a stainless steel autoclave and heated to 190 °C using a ramping rate of 1 °C/min. The reaction temperature was maintained at 190 °C for 4 h. The autoclave was the left to cool to ambient temperature. The suspension was recovered and washed several times with ethanol and then water. The product was left overnight in an oven at 90 °C. To further purify the product, a Soxhlet extraction method was used to remove polyaromatic hydrocarbons (PAHs) from the carbon spheres using toluene as the solvent. After the extraction, the spheres were dried again overnight at 90 °C.

2.2 Annealing of the UN-CSs-H

The carbon spheres prepared were subjected to a further heat treatment under inert (N_2) conditions. To carry out the annealing experiment, about 3 g of the as-prepared carbon spheres were placed in a quartz boat in a quartz tube. The boat and its content were placed in the middle of a quartz tube reactor and the reactor was inserted into a furnace. Nitrogen (flow rate of 20 mL/min) was passed through the reactor while the temperature was ramped at 10 °C/min to 900 °C left for 4 h and then cooled. This material was labelled as CSs-H.

2.3 Functionalization of CSs

The annealed CSs-H (1.5 g) was added to 100 mL of 55% HNO_3. The suspension was then stirred and refluxed at 110 °C for 2.5 h. The product was washed with a large amount of distilled water until the pH attained a neutral value (pH 7). It was then left in the oven overnight at 100 °C and this was labelled F-CSs-H.

2.4 Catalyst Preparation

Two different catalyst preparation methods were employed in this study. A set of Ru catalysts were made by adding Ru to the un-functionalized and functionalized supports (CSs-H and F-CSs-H) respectively using the impregnation method. This was achieved by dropwise addition of the desired amount of $RuCl_3$ in water to the support to achieve a 5 wt% Ru loading. The materials were labelled as CSs-HIMP and F-CSs-HIMP.

Another catalyst was prepared by the microwave irradiation polyol method. The $RuCl_3$ solution and the F-CSs-H was dispersed in ethylene glycol and sonicated for 15 min. The Ru mixture obtained was added dropwise to the F-CSs-H (1 g) and the reaction content transferred into Teflon vessels and then placed in the microwave oven. In the polyol synthesis method, the reaction involves the oxidation of the solvent ethylene glycol into glycolic acid which is preceded by oxidation to an aldehyde intermediate. Reduction of metallic ions to their elemental state then proceeds following decomposition of the ethylene glycol (120–160 °C). Microwave heating of a polyol solution has also been used for the reduction of a metal salt. Microwave irradiation is believed to favour dehydrogenation of the aldehyde intermediate which plays a critical role in the reduction of the metallic salt. This arises because of the high reduction ability as well as high dielectric losses of ethylene glycol. Generally, microwave irradiation offers significant advantages over conventional heating. This includes, homogeneous nucleation as a result of uniform heating, very short thermal induction periods and shorter crystallization times. Localized high temperatures generated at reaction sites also enhances the reduction rate of metallic salts and usually super heating above the solvent's boiling point occurs due to the microwave dissipation over the whole liquid volume. Due to the above mentioned advantages, microwave dielectric loss heating is a good option for a synthesis process in view of its energy efficiency, time saving, lack of thermal convection and simplicity. The poloyol sample was labelled F-CSs-HMIC. All catalysts with ruthenium contained 5 wt% of the metal and all were calcined at 220 C prior to use.

2.5 Catalyst Testing

The methanation reactions were carried out in a fixed bed tubular reactor (FBTR). A K-type thermocouple was employed to monitor the temperature in the fixed bed. The methanation gases (99.99%) were fed into the reactor chamber from gas cylinders (for CO methanation: 1% CO, 10% N_2 and H_2 balance; for selective CO methanation: 1% CO, 20% CO_2, 10% N_2 and H_2 balance; and for CO_2 methanation: 20% CO_2, 10% N_2 and H_2). The catalyst (1 g) was typically reduced in situ using hydrogen gas (99.995% purity)

at 250 °C for 3 h at 1 bar. For all the methanation reactions, the temperatures ranged between 100 and 360 °C. The gas flow rate was kept at 150 mL/min for all the reactions. An online gas chromatograph (GC) equipped with Porapak Q and Carboxen-1000 columns coupled to a FID and a TCD were used to monitor the outlet gas composition.

2.6 Characterization

The surface areas of all the catalysts and supports were analysed by BET using N_2 physisorption (Micromeritics ASAP-2000 Tri-star analyser). Before the surface area analysis, 0.2 g of the sample was degassed for 6 h at 150 °C under a N_2 flow using a Micromeritics flow Prep 060. The weight losses of the carbon samples were monitored on a Perkin-Elmer STA6000 TG/DTA Thermogravimetric analyser. The analyses were performed in air at a heating rate of 10 °C/min.

The morphologies of the samples were identified using SEM (FEI Nova Nanolab 600) and TEM (Tecnai T12) images. TEM samples were prepared by dispersing the catalyst in ethanol followed by sonication for 2 min. A drop of the ethanol suspension was transferred to a copper grid and dried. The disorder in the carbon-based supports were measured with a micro-Raman attachment of a Jobin-Yvon T64000 Raman spectrometer. The excitation wavelength was 514.5 nm from an Ar ion laser and the spot size on the sample was ca. 1.5 μ in diameter.

TGA analysis of the as-synthesized and CSs-H and F-CSs-H were conducted in a TGA-4000 (Perkin Elmer) analyser equipped with Pyris software. The analyses were done in air to ascertain the degree of functionalization. Approximately 10 mg of the sample was placed in the sample holder and air (flow rate of 20 mL/min) was flowed over the sample. The samples were heated to 900 °C at a heating rate of 10 °C/min from 35 °C.

The reducibility of the Ru was studied using H_2-TPR and carried out using a Micromeritics Autochem 2910 instrument. Typically, 0.15 g of the catalyst was loaded into a U-shaped quartz tubular reactor. The reactor was heated to 150 °C under an argon atmosphere at a heating rate of 5 °C/min for 30 min and then cooled to 50 °C. The TPR analysis was performed by exposing the catalyst to 5% H_2, (balance Ar) at a flow rate of 40 mL/min while heating at a rate of 5 °C/min to 900 °C. Any change in the amount of H_2 flowing through the reactor and the reference was observed using a TCD.

A Micromeritics Autochem 2910 instrument was used to conduct chemisorption experiments. The samples were first degassed in situ at 150 °C for 30 min. The samples were further reduced with H_2 (99.999% purity) at 250 °C for 2 h and cooled to an ambient temperature under helium gas. The pulsing experiments were carried out with a 423 μL sample loop filled with a mixture of helium and H_2 (99.999% purity). The sample temperature was held at 70 °C in the reactor and then the gas was injected for adsorption to take place. The percentage metal dispersion and the mean Ru crystallite size were calculated based on the H_2 uptake assuming a H_2:Ru stoichiometry of 1:2 [40]. The Ru crystallites were assumed to be spherical in all cases and calculated from the relation below:

$$d_M = \frac{6 \times 102 \times \mathrm{MW}}{\rho_M \times \vartheta_M \times 6.022 \times 10^{23} \times D} \quad (5)$$

where d_M is the mean crystallite size, MW is the atomic mass for Ru (101.07 g mol^{-1}), ρ_M is the Ru density (12.3 g cm^{-3}), ϑ_M is the exposed surface area per gram of Ru metal and D is the percentage dispersion of the Ru metal [40]

3 Results and Discussion

3.1 Support Characterization

Insight into the morphology of the hydrothermally synthesized CSs was gained through TEM analysis. Figure 1 shows the TEM images and size distribution graph for the synthesized CSs after a Soxhlet extraction procedure and annealing at 900 °C. It was observed that the carbon materials were spherical in shape and consisted of sizes ranging from 300 to 1000 nm with an average size of 650 nm as show in the size distribution graph in Fig. 1c. They appeared to be monodispersed (Fig. 1a, b) but showed a necklace like accreted conformation. Their surface morphology changed after annealing, consistent with earlier reports by Dlamini and Kumi who showed that the CS surface roughened, due to removal of polymeric species and this led to the opening of the pore structure [33].

3.2 Nitrogen Adsorption–Desorption

Nitrogen physisorption studies were performed on the annealed CSs-H sample (functionalized and un-functionalized). A comparison of the two adsorption–desorption isotherms and pore size distributions are presented in Fig. 2 and Table 1. Both samples exhibited micro and mesopores (type 4 according to the IUPAC classification) and a sharp capillary condensation occurred between 0.4 and 0.6 relative pressure. Interestingly, the functionalized (annealed) sample displayed a relatively higher N_2 adsorption at lower relative pressure (p/p_o) and a larger hysteresis loop (at $p/p_o = 0.4–0.9$) than the un-functionalized CSs-H. The hysteresis curve loops confirm the presence of well-defined mesopores. In addition to the larger hysteresis loop (Fig. 2a, b), a higher pore volume (0.31 cm^{-3} g^{-1}) and average pore diameter

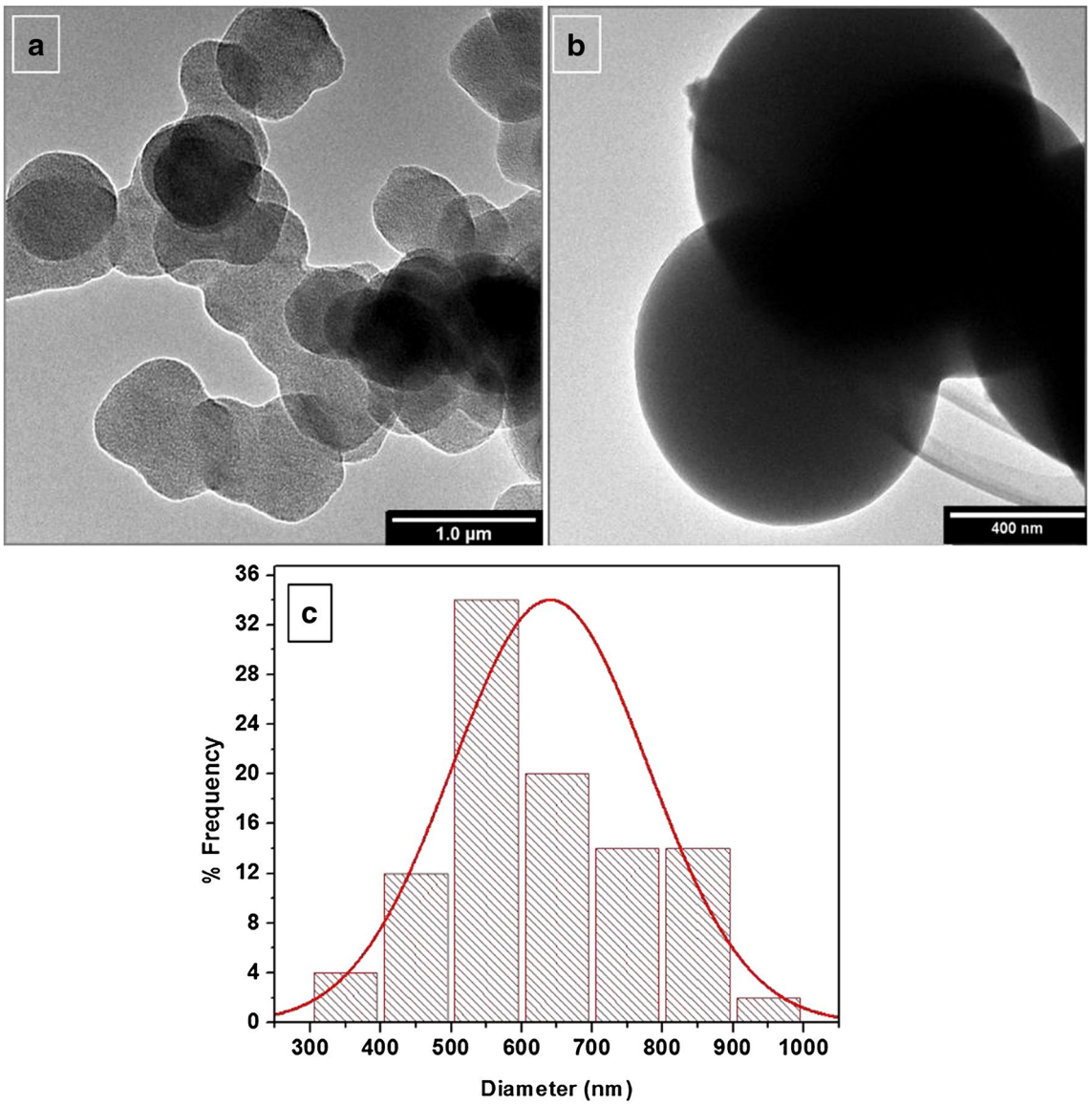

Fig. 1 TEM images (**a, b**) and (**c**) size distribution graph of the hydrothermally synthesized carbon spheres

(4.5–6.5 nm) was also observed for the functionalized CSs-H compared to the un-functionalized CSs-H (0.21 cm^{-3} g^{-1}; 3.1–3.9 nm) as shown in Fig. 2c, d. This implied that functionalizing the CSs-H created more and larger pores. This led to the higher surface area (509 m^2 g^{-1}) when compared to the un-functionalized CSs-H (463 m^2 g^{-1}) (Table 1).

3.3 Raman Spectral Analysis

The graphitic order in the carbon frame work was measured using Raman spectroscopy. In Fig. 3, the Raman spectra of the functionalized and un-functionalized (annealed) CSs-H were compared. The in-plane vibration of the sp^2 carbon atom indicated a G-band (at 1590 and 1595 cm^{-1}) whereas the D-band characterized a defect-induced Raman feature, representing the degree of non-perfect crystalline structures (at 1344 and 1350 cm^{-1}). The analysis of the band intensities (D vs. G, I_D/I_G) gives information about bond features in the carbon framework. An increase in the I_D/I_G ratio was observed when the annealed sample was functionalized, and this is consistent with a higher defect content as a result of the acid treatment [31, 41]. This result agrees with the BET data (Table 1).

3.4 Thermogravimetric Analysis (TGA)

Thermogravimetric analysis profiles of the carbon spheres are shown in Fig. 4. The measurements were carried out under an oxidizing atmosphere. Notably, the un-functionalized sample which demonstrated a higher graphitic nature,

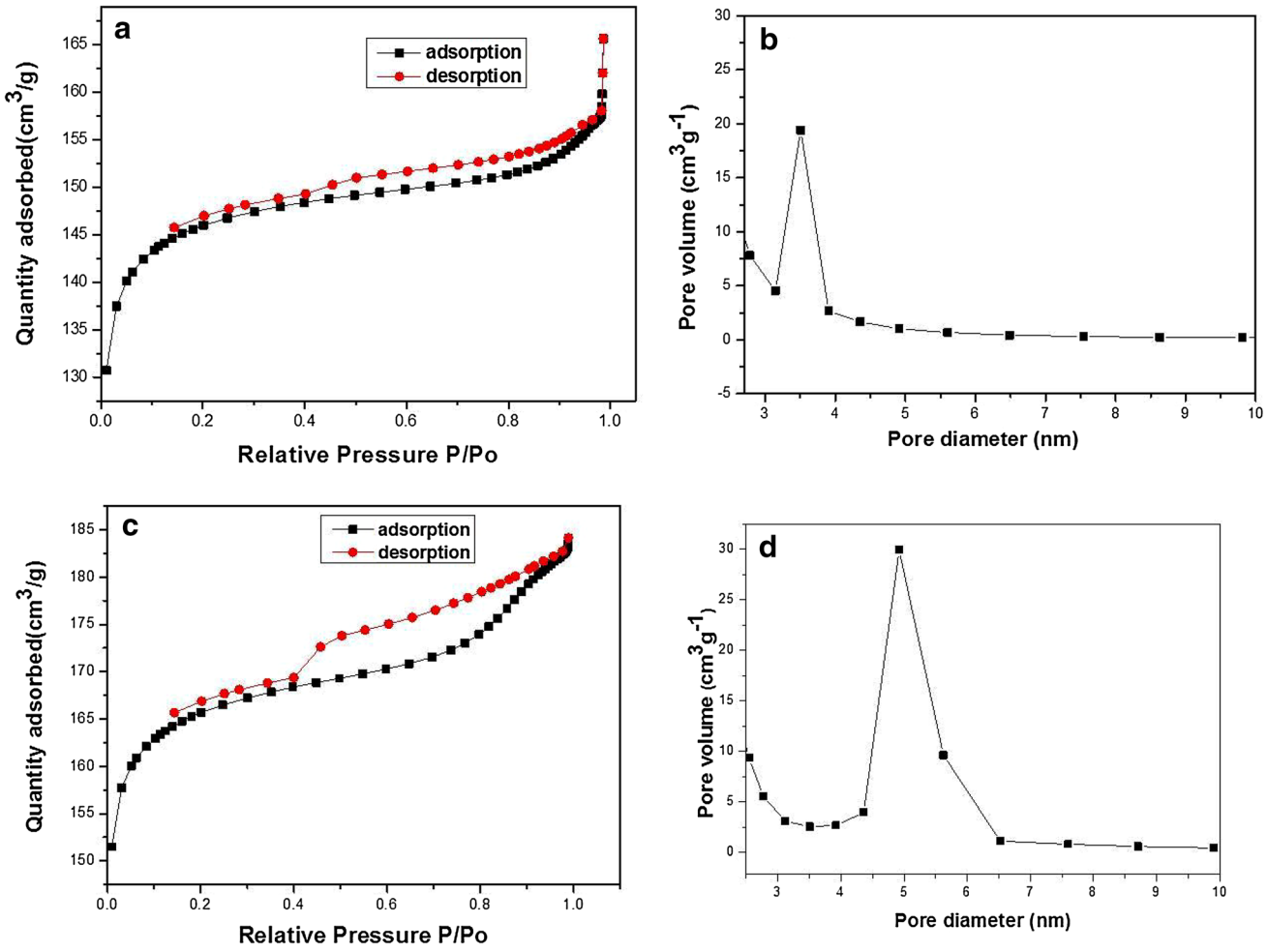

Fig. 2 N_2 adsorption–desorption isotherms and pore size distribution plots for functionalized (**a, b**) and un-functionalized CSs-H (**c, d**)

Table 1 Properties of the CSs-H

Analysis	F-CSs-H	CSs-H
BET ($m^2\ g^{-1}$)	509	463
Pore volume ($cm^3\ g^{-1}$)	0.31	0.21
Pore diameter (nm)	4.9	3.5
D-band (cm^{-1})	1351	1344
G-band (cm^{-1})	1595	1590
I_D/I_G	0.96	0.69
Decomposition temp (°C)[a]	578	661

[a]In air from TGA analysis

from Raman studies, also showed good thermal stability with complete decomposition at T > 600 °C. In contrast the F-CSs-H sample oxidized completely at T < 600 °C. This implied that acid treatment which introduced oxygen containing functional groups compromised the CSs-H thermal stability. The removal of the functional groups on the surface of the carbon spheres led to the shape of the curve seen in

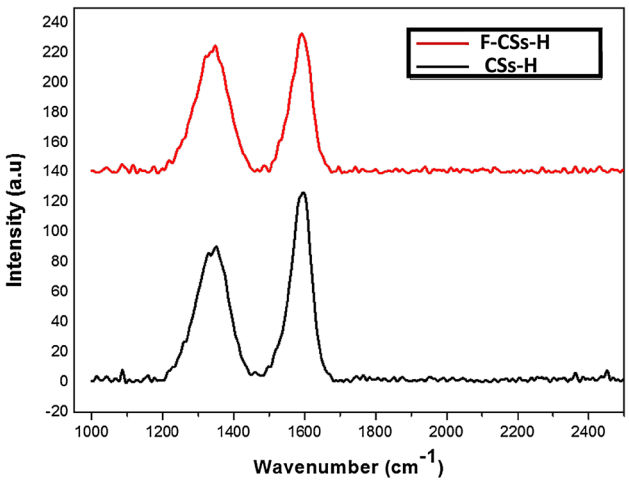

Fig. 3 Raman spectra of the functionalized and un-functionalized CSs-H

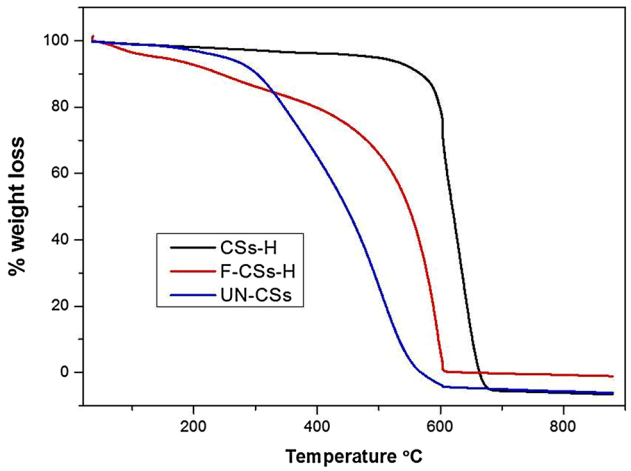

Fig. 4 TGA plots showing functionalized, un-functionalized and un-annealed SCs-H

Fig. 4. The data for the un-annealed sample was added to the TGA plots for comparison (Fig. 4). The derivative weight loss plots are presented in Fig. S1. It was observed that the un-annealed sample contained some polymeric materials after the Soxhlet extraction.

3.5 Catalyst Characterization

Figure 5 shows TEM images of the Ru nanoparticle catalysts supported on CSs-H made by the three different procedures. The Ru size distributions are also shown in Fig. 5. The catalyst prepared by the microwave polyol technique gave fairly small RuO_2 particles ($d = 2.7$ nm) which were relatively well dispersed on the support (Fig. 5a). The size distribution graph indicated the particles had a narrow size distribution. This shows that the microwave technology offered good control over the size of the Ru particles using the selected conditions for the preparation of the catalyst. Again, functionalizing the solid spheres created defects in the carbon framework and the sample had oxygenated functional groups that allowed the RuO_2 to bind to the supports. The Ru impregnated on the acid treated support (FCSs-HIMP) gave RuO_2 particles with an average particle size of 3.4 nm. The RuO_2 had a slightly wider size distribution compared to the microwave prepared catalyst as indicated in the particle size distribution graph in Fig. 5b. The absence of functional groups and defect content for the CSs-HIMP resulted in the synthesis of relatively larger RuO_2 particles ($d = 10.2$ nm) with a significantly wider size distribution range (Fig. 5c). The particles might also have sintered during the calcination process due to the absence of functional groups to aid in binding the particles.

Table 2 summarizes both the physical and chemical properties of the different Ru catalysts supported on carbon spheres. The surface areas for all the catalysts are reduced after loading with Ru. This was largely due to blocking of the mesopores by the Ru metal particles. Marginal pore volume reduction in this catalyst was noted. The catalyst prepared using the microwave polyol method generated smaller Ru particles hence resulting in a higher dispersion (64%). The larger Ru particles observed on the un-functionalized CSs-H were poorly dispersed and this was confirmed by the chemisorption data as shown in Table 2. The impregnated catalyst supported on functionalized CSs-H had a relatively higher dispersion for the Ru particles.

3.6 TPR Studies

The different catalysts were subjected to reduction studies (Fig. 6) and all the reduction reactions occurred between a temperature range of 100–119 °C. Reduction from RuO_2 to Ru occurred at different maximum temperatures for the different supported catalysts, indicating that both support and the catalyst preparation method influenced the reduction of the active metal. From the graphs, the reduction of RuO_2 to Ru occurred at a higher temperature on the functionalized supports compared to reduction on the un-functionalized supported catalyst. This was attributed to the weakly bound RuO_2 on the un-functionalized support due to the absence of functional groups. The F-CSs-HIMP with larger RuO_2 particles reduced at a relatively higher temperature and in a wider temperature range when compared to the smaller and uniform RuO_2 particles generated by the microwave irradiation technique. No significant strong metal support interaction (SMSI) was observed implying that the functional groups did not form strong chemical bonds between the support and the Ru. The reduction profile revealed that the nature of the surface of the support and the size of the particles played a role in terms of the maximum reduction temperature and width of the peaks. The broad peaks observed between 300 and 600 °C are due to carbon reduction to form methane [37].

3.7 CO Methanation

Figure 7 shows the behaviour of the three Ru catalysts on the CSs-H as support for the CO hydrogenation reaction. As expected, increasing temperature resulted in an increased CO conversion. All the catalysts completely converted CO within a temperature range of 240–300 °C. The surface of the CSs-H support, modified by acid functionalization, introduced oxygenated groups that correlated with the CO methanation activity. It can be observed from the conversion plots (Fig. 7) that, both CSs-HIMP and CSs-HMIC displayed significantly higher activity when compared to the un-functionalized (CSs-H). From the Raman studies, it was confirmed that acid treatment

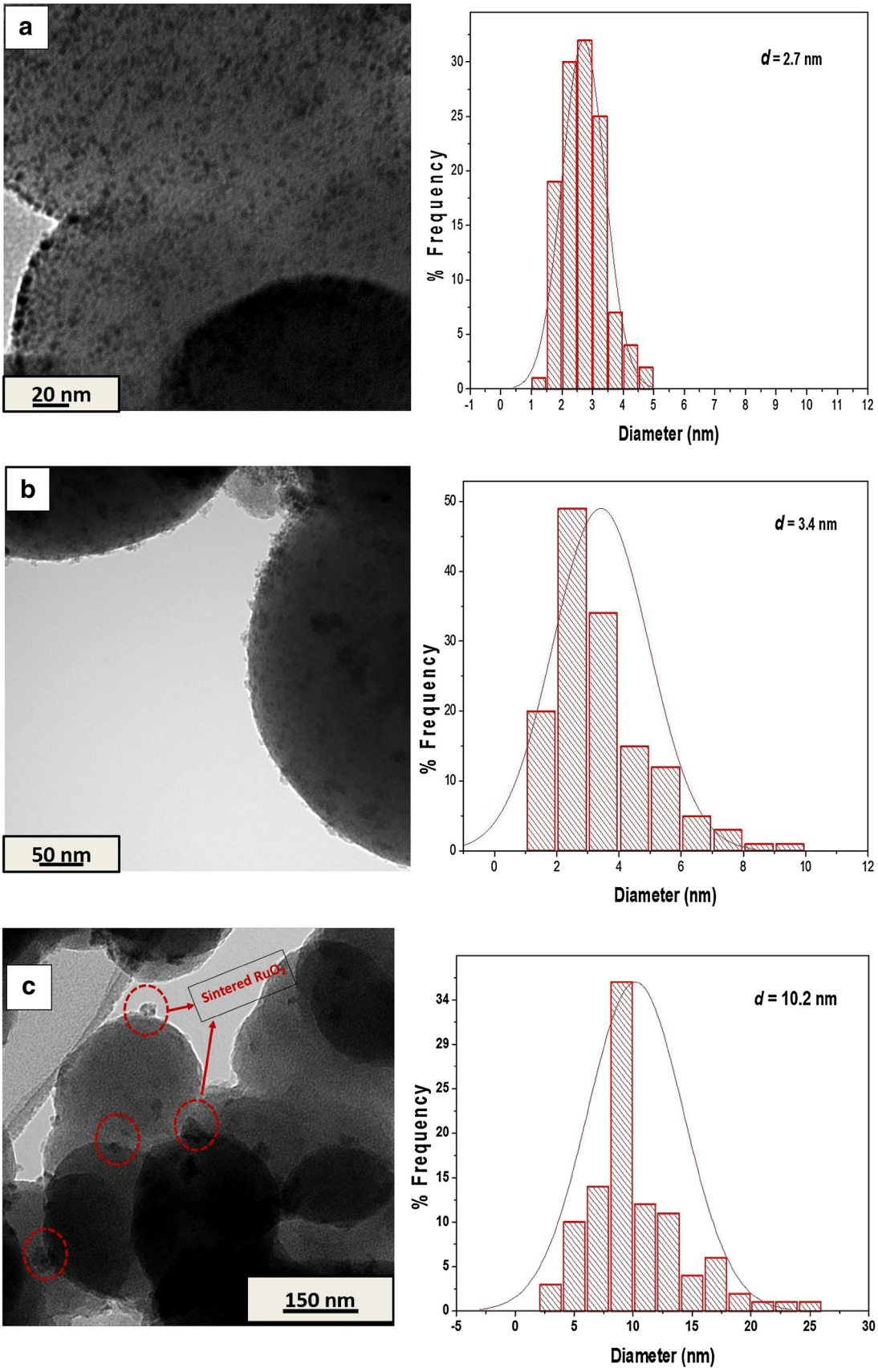

Fig. 5 Ru catalyst supported SCs-H **a** F-SCs-HMIC, **b** F-SCs-HIMP and **c** SCs-HIMP

Table 2 Physicochemical properties of the catalysts

Sample	BET ($m^2\ g^{-1}$)[a]	Pore volume ($cm^3\ g^{-1}$)	d_{RuO_2} (nm)[b]	d_{Ru} (nm)[c]	Dispersion (%)
SCs-HIMP	443	0.21	10.2	5.9	17
F-SCs-HIMP	468	0.28	3.4	2.2	56
F-SCs- HMIC	471	0.29	2.7	1.8	64

[a]Surface area BET

[b]RuO_2 from TEM

[c]Ru from H_2 chemisorption

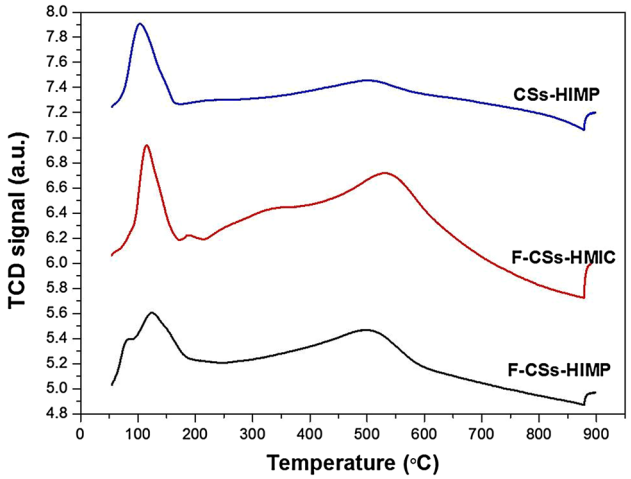

Fig. 6 Temperature programmed reduction plots for the different catalysts

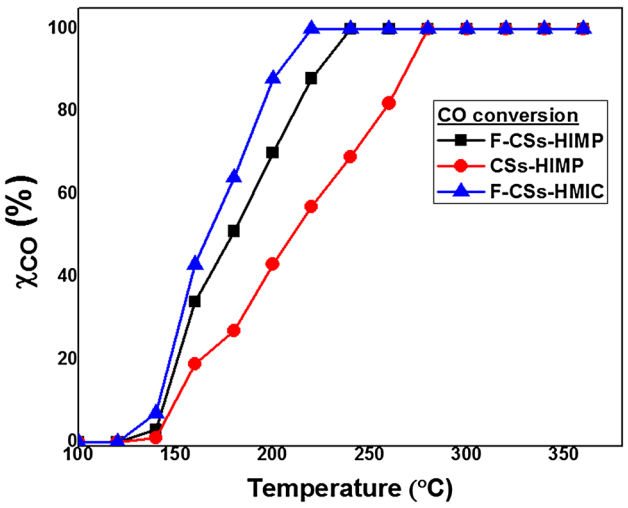

Fig. 7 The effect of temperature on the CO conversion (X_{CO}) as a function of reaction temperature using 5 wt% Ru. Experimental conditions: mass of catalyst: 1 g; reactant composition: 1% CO, 89% H_2 (balance N_2); total flow rate: 150 $cm^3\ min^{-1}$

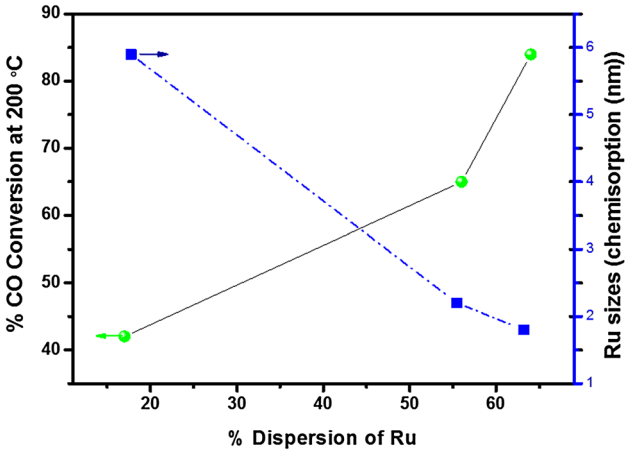

Fig. 8 Dependence of CO methanation activity and particle size as a function of Ru dispersion

modified the surface and increased the defects in the support material. The BET data also revealed a higher surface area as well as a higher mesopore volume after acid treatment of the support. This effect is believed to increase anchorage sites for the Ru particles. Also, the oxygenated functional groups helped stabilize the Ru particles against sintering under mild heat treatment conditions [37, 39, 41, 42]. The improved dispersion of Ru species on the support is seen in the chemisorption data (Table 2). This explains the higher activity recorded.

From the plots in Fig. 7, it can be seen that the microwave irradiation polyol technique which generated relatively smaller, narrower and uniformly dispersed Ru particles gave the best data. The microwave catalyst preparation indicated that the method provided for good control over the size and size distribution of the Ru. This clearly suggests that the microwave polyol technique is appropriate for preparing laboratory scale catalysts with small diameters.

Data for the CO methanation activity at 200 °C are shown in Fig. 8. Overall, the methanation activity i.e. conversion data increased with the ruthenium dispersion.

3.8 Methane Selectivity

Methane dominated as the major product for the CO hydrogenation process at temperatures above 240 °C as shown in Fig. 9. It was noted that some other higher hydrocarbons were produced at lower temperatures. The un-functionalized supported catalyst with larger Ru particles produced other hydrocarbons besides methane at lower temperature. The main product formed below 240 °C over F-SCs-HMIC besides CH_4 was C_2H_6 (15% at 160 °C), while CSs-HIMP gave about 0.4% C_3H_8 at 160 °C in addition to C_2H_6. Similar results have been reported in previous studies by Jiménez et al. when they studied the nature of carbon fiber supported Ru as an active catalyst [27].

3.9 CO_2 Methanation

CO_2 methanation was also studied with the three different catalysts using similar experimental conditions to those used in the CO methanation reaction. The results are presented in Fig. 9 and shows that the CO_2 conversion was less than 40% over the total range of temperatures studied. The catalysts prepared with the functionalized support using Ru added by impregnation or microwave routes had almost similar conversions. This indicated that the catalyst preparation had little effect on CO_2 activity. The CSs-HIMP catalyst was practically inactive below 250 °C. A conversion above 10% occurred at 320 °C which implied that the support affected this reaction (Fig. 10)

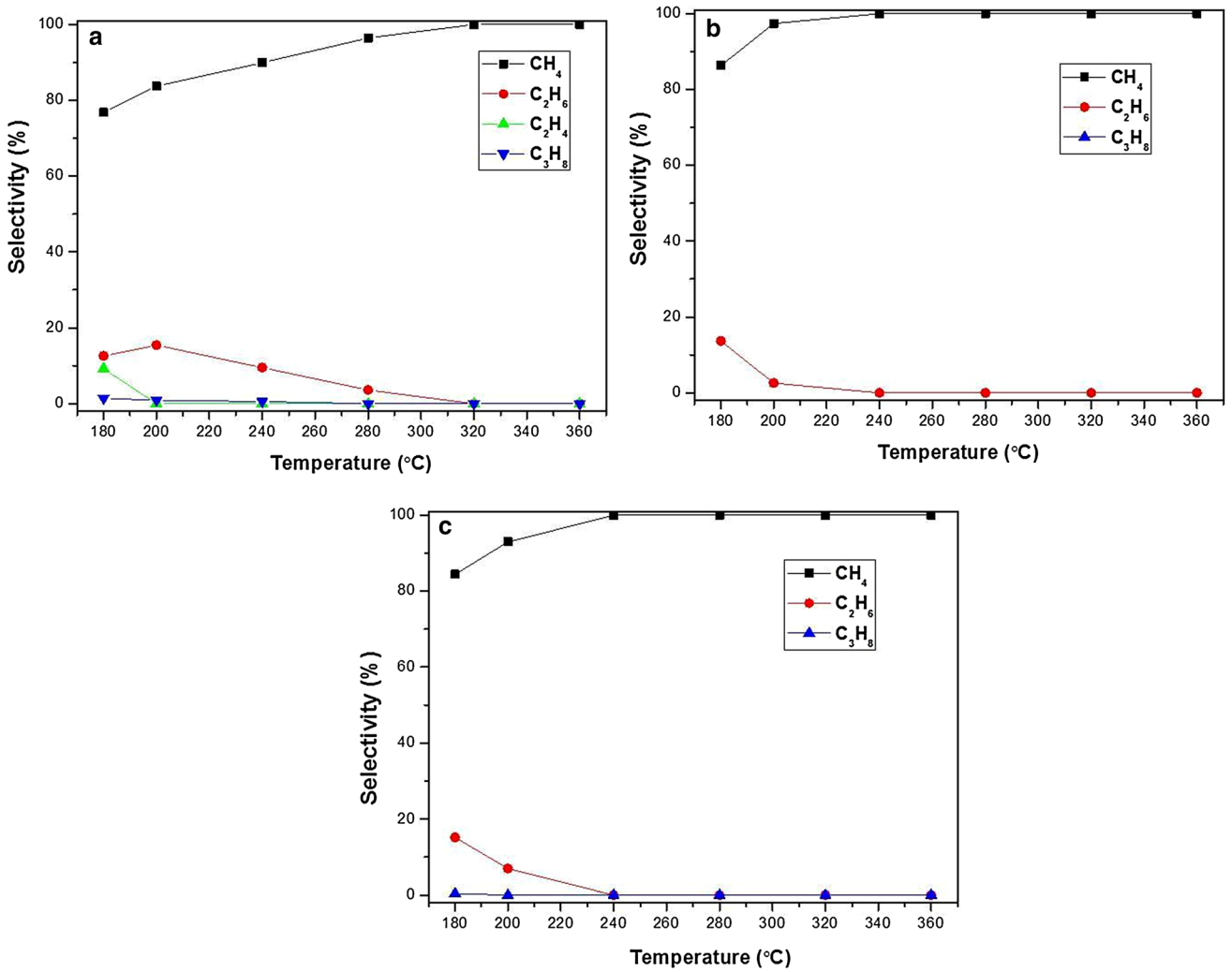

Fig. 9 The effect of reaction temperature on the selectivity of **a** CSs-HIMP, **b** F-CSs-HMIC and **c** F-CSs-HIMP catalysts

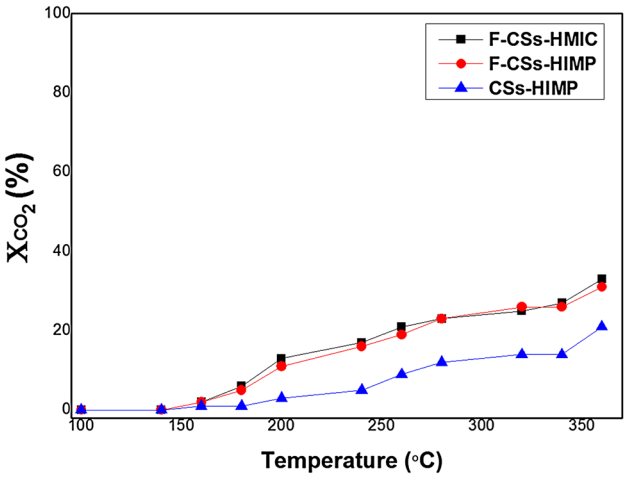

Fig. 10 The effect of temperature on the CO_2 conversion (X_{CO}) CSs-H as a function of reaction temperature using 5 wt% Ru. Experimental conditions: mass of catalyst: 1 g; reactant composition: 1% CO, 89% H_2 (balance N_2); total flow rate: 150 cm^3 min^{-1}

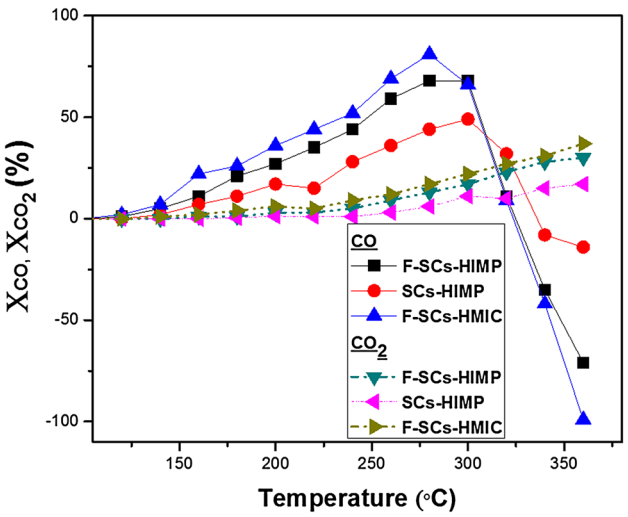

Fig. 11 The effect of CSs-H support on catalytic performance **a** CO conversion (X_{CO}) and **b** selective methanation of CO in the presence of CO_2 (X_{CO_2}) as a function of reaction temperature using 5 wt% Ru. (Solid lines: CO conversion: broken lines: CO_2 conversion). Experimental conditions: mass of catalyst: 1 g; reactant composition: **a** 1% CO, 89% H_2 (balance N_2) and **b** 1% CO, 20% CO_2, 69% H_2 (balance N_2); total flow rate: 150 cm^3 min^{-1}

3.10 Selective CO Methanation

The different catalysts were studied under selective CO methanation conditions in the presence of excess CO_2 (Fig. 11). The functionalized supported catalysts displayed higher activity as seen for CO methanation in the absence of CO_2. This can be explained, as before, for CO methanation. None of the catalysts attained 100% CO conversion under the selective methanation conditions employed.

The CO output for all the catalysts (Fig. 11) dropped after they attained their maximum conversion between 280 and 300 °C. This was due to the formation of CO produced by CO_2 [27]. This reaction, the RWGS, runs parallel with the CO methanation process. The un-functionalized supported Ru catalyst showed the lowest CO conversion. However, the RWGS reaction for the un-functionalised CS-H was less significant when compared to the functionalized Ru supported catalyst i.e. the maximum % CO generated in the effluent at 360 °C (the maximum temperature studied) in the selective CO methanation reactions were, 98%, 71% and 14% for F-CSs-HMIC, F-CSs-HIMP and CSs-HIMP catalysts. Overall, functionalisation led to an over threefold increase in Ru dispersion. As mentioned in the introduction, some studies have suggested that CO_2 interacts with the surface support which leads to carbonate specie formation on the support. The formate species bordering the active metal are then decomposed into CO within the metal-support interface leaving the residual species [35, 38]. This suggests that the presence of oxygenated functional groups, especially OH groups which have been confirmed to be present on functionalized carbon materials [37, 38, 42, 43] on the supports aided both CO_2 conversion [34, 35] and promoted the RWGS reaction under the experimental condition employed. This is in agreement with our previous work where surface functional groups on CNTs were covered with TiO_2 and this coverage of the functional groups retarded the WRGS reactions significantly [44].

4 Conclusions

The hydrothermally synthesized solid carbon spheres functionalized with HNO_3 recorded a significant increase in the specific surface areas resulting from the modification of the support by acid treatment. These particles improved the dispersion of the Ru when compared to the un- functionalized support. The microwave polyol catalyst preparation technique resulted in the formation of small uniformly sized Ru particles dispersed on the support.

The un-functionalized carbon had poorly dispersed large Ru particles with a wide size range distribution with poor CO conversion. Despite this drop in CO conversion, the catalyst recorded the lowest reverse water gas shift activity which generated extra CO in the reformate gas feed. This was explained as due to the absence of OH functional groups on the support which should enhance associative adsorption of CO_2. A very small percentage of higher hydrocarbons (mostly C_2H_6) were observed at lower temperatures when the CO conversions were below 10%.

The conversion for both CO and CO_2 methanation reactions increased with increasing ruthenium dispersion i.e. decreased with Ru particle size.

Acknowledgements The authors express thanks to the National Research Foundation and the University of the Witwatersrand for financial support of this work.

Compliance with Ethical Standards

Conflict of interest The authors declare that they have no conflict of interest.

References

1. Chen A, Miyao T, Higashiyama K, Yamashita H, Watanabe M (2010) Angew Chem Int Ed 49:9895
2. Choudhury MBI, Ahmed S, Shalabi MA, Inui T (2006) Appl Catal A 314:47
3. Kimura M, Miyao T, Komori S, Chen A, Higashiyama K, Yamashita H, Watanabe M (2010) Appl Catal A 379:182
4. Jian L, Botao Q, Jingyue L, Yanqiang H, Aiqin W, Lin L, Wansheng Z, Xiaodong ALFW, Tao Z (2012) Angew Chem Int Ed 51:2920
5. Kandoi S, Gokhale AA, Grabow LC, Dumesic JA, Mavrikakis M (2004) Catal Lett 93:93
6. Guan H, Lin J, Li L, Wang X, Zhang T (2016) Appl Catal B 184:299
7. Dagle RA, Wang Y, Xia GG, Strohm JJ, Holladay J, Palo DR (2007) Appl Catal A 326:213
8. Dudfield CD, Chen R, Adcock PL (2001) Int J Hydrog Energy 26:763
9. Krämer M, Duisberg M, Stöwe K, Maier WF (2007) J Catal 251:410–422
10. Takenaka S, Shimizu T, Otsuka K (2004) Int J Hydrog Energy 29:1065
11. Oh SH, Sinkevitch RM (1993) J Catal 142:254
12. Xu G, Chen X, Zhang ZG (2006) Chem Eng J 121:97
13. Bessell S (1993) Appl Catal A 96:253
14. Iglesia E, Soled SL, Fiato RA (1992) J Catal 137:212
15. Reuel RC, Bartholomew CH (1984) J Catal 85:78
16. Tan H, Li K, Sioud S, Cha D, Amad MH, Hedhili MN, Al-Talla ZA (2012) Catal Commun 26:248
17. Xu L, Song H, Chou L (2011) Catal Sci Technol 1:1032
18. Cai W, Yu J, Anand C, Vinu A, Jaroniec M (2011) Chem Mater 23:1147
19. Li L, Niu S, Qu Y, Zhang Q, Li H, Li Y, Zhao W, Shi J (2012) J Mater Chem 22:9263
20. Li ZX, Shi FB, Li LL, Zhang T, Yan CH (2011) Phys Chem Chem Phys 13:2488
21. Morris SM, Fulvio PF, Jaroniec M (2008) J Am Chem Soc 130:15210
22. Xu L, Song H, Chou L (2013) Int J Hydrog Energy 38:7307
23. Bahome MC, Jewell LL, Hildebrandt D, Glasser D, Coville NJ (2007) Appl Catal A 287:60
24. Bahome MC, Jewell LL, Padayachy K, Hildebrandt D, Glasser D, Datye AK, Coville NJ (2007) Appl Catal A 328:243
25. Bezemer GL, Bitter JH, Kuipers HP, Oosterbeek H, Holewijn JE, Xu X, Kapteijn F, van Dillen AJ, de Jong KP (2006) J Am Chem Soc 128:3956
26. Chen W, Fan Z, Pan X, Bao X (2008) J Am Chem Soc 130:9414
27. Jiménez V, Sánchez P, Panagiotopoulou P, Valverde JL, Romero A (2010) Appl Catal A 390:35
28. Lv R, Cui T, Jun MS, Zhang Q, Cao A, Su DS, Zhang Z, Yoon SH, Miyawaki J, Mochida I (2011) Adv Funct Mater 21:999
29. Tavasoli A, Trépanier M, Abbaslou RMM, Dalai AK, Abatzoglou N (2009) Fuel Process Technol 90:1486
30. Trépanier M, Tavasoli A, Dalai AK, Abatzoglou N (2009) Appl Catal A 353:193
31. Mhlanga SD, Coville NJ (2008) Diam Relat Mater 17:1489
32. Deshmukh AA, Mhlanga SD, Coville NJ (2010) Mater Sci Eng R 70:1
33. Dlamini MW, Kumi DO, Phaahlamohlaka TN, Lyadov AS, Billing DG, Jewell LL, Coville NJ (2015) ChemCatChem 7:3000
34. Tada S, Kikuchi R, Urasaki K, Satokawa S (2011) Appl Catal A 404:149
35. Tada S, Kikuchi R (2015) Catal Sci Technol 5:3061
36. Marwood M, Doepper R, Renken A (1997) Appl Catal A 151:223
37. Motchelaho MA, Xiong H, Moyo M, Jewell LL, Coville NJ (2011) J Mol Catal A 335:189
38. Phao N, Nxumalo EN, Mamba BB, Mhlanga SD (2013) Phys Chem Earth A/B/C 66:148
39. Xiong H, Moyo M, Motchelaho MA, Tetana ZN, Dube SMA, Jewell LL, Coville NJ (2014) J Catal 311:80
40. Gonzalez CJM, Finocchio E, Garcia S, Rojas S, Ojeda M, Busca G, Fierro JLG (2011) Catal Sci Technol 1:1013
41. Tetana ZN (2013) Boron and nitrogen doped carbons for photochemical degradation reactions. PhD thesis, The University of the Witwatersrand, Johannesburg
42. Ayala P, Arenal R, Rümmeli M, Rubio A, Pichler T (2010) Carbon 48:575
43. Graham U, Dozier A, Khatri R, Bahome M, Jewell L, Mhlanga S, Coville N, Davis B (2009) Catal Lett 129:39
44. Kumi DO, Phaahlamohlaka TN, Dlamini MW, Mangezvo IT, Mhlanga SD,. Scurrell MS, Coville NJ (2018) Appl Catal B 232:492

Affiliations

David O. Kumi[1] · Mbongiseni W. Dlamini[1] · Tumelo N. Phaahlamohlaka[1] · Sabelo D. Mhlanga[2] · Neil J. Coville[1] · Mike S. Scurrell[3]

✉ Neil J. Coville
neil.coville@wits.ac.za

✉ Mike S. Scurrell
scurrms@unisa.ac.za

[1] School of Chemistry, Molecular Sciences Institute, University of the Witwatersrand, PO WITS, Johannesburg 2050, South Africa

[2] Nanotechnology and Water Sustainability Research Unit, College of Science, Engineering and Technology, University of South Africa, Florida, Johannesburg 1710, South Africa

[3] Department of Civil and Chemical Engineering, University of South Africa, Florida 1710, South Africa